Structure-property relationships in cubic cuprous iodide: A novel view on stability, chemical bonding, and electronic properties

A. Pishtshev[1] and S. Zh. Karazhanov[2]

[1]*Institute of Physics, University of Tartu, 50411 Tartu, Estonia*

[2]*Department for Solar Energy, Institute for Energy Technology, 2027 Kjeller, Norway*

ABSTRACT

Based on the combination of computational DFT and theory-group methods, we performed systematic modeling of γ-CuI structural design at the atomistic level. Being started from the metallic copper lattice, we treated a crystal assembly as a step-wise iodination process characterized in terms of a sequence of intermediate lattice geometries. These geometries were selected and validated via screening of possible structural transformations. The genesis of chemical bonding was studied for three structural transformations by analyzing the relevant changes in topology of valence electron densities. We determined structural trends driven by metal-ligand coupling. This allowed us to suggest the improved scenario of chemical bonding in γ-CuI. In particular, the unconventional effect of spatial separation of metallic and covalent interactions was found to be very important with respect to the preferred arrangements of valence electrons in the iodination process. We rigorously showed that useful electronic and optical properties of γ-CuI origin from the combination of two separated bonding patterns -- strong covalency established in I-Cu tetrahedral connections and noncovalent interactions of copper cores caused by the $3d^{10}$ closed-shell electron configurations. The other our finding is that the self-consistency of the GW calculations is crucial for correct determining the dynamic electronic correlations in γ-CuI. Detail reinvestigation of the quasi-particle energy structure by means of the self-consistent GW approach allowed us to explain how *p*-type electrical conductivity can be engineered in the material.

KEYWORDS: Cuprous iodide, transparent conducting film, DFT calculations, hole transport layer, covalent bonding, point defect, Cu-Cu bonding.

1. INTRODUCTION

A number of wide band gap semiconductors possessing p-type electrical conductivity has attracted extensive research attention due to important applications in semiconducting electronic devices. One of such applications takes place in photovoltaic technology where the *p*-type wide band gap semiconductor is employed as a hole transport layer in perovskite solar cells. Great possibilities for the integration with the perovskite architecture of an optoelectronic device have been demonstrated by cuprous iodide (CuI). It represents a low cost inorganic material, possessing the wide band gap Eg=3.1 eV, stable *p*-type electrical conductivity at room temperature and fast ionic conductivity at high temperatures [1]. The crystal chemistry of the solid CuI is characterized by three structural phases α, β and γ differing each from other by thermal stability. Under ambient conditions CuI crystallizes into the zinc-blende structure (γ-phase), while the cubic α- and hexagonal β-phases are high-temperature [1-5]. The main technological interest to γ-CuI is caused by the useful combination of good intrinsic electrical conductivity and optical transparency with respect to the visible light, and by a possibility to tune its electrical conductivity through the preparation and synthesis conditions [1]. Prominent examples which illustrate the successful utilization of γ-CuI as the hole transport layer are the solid-state dye-sensitized and perovskite solar cells [6-7]. In the anthracene-containing PPE-PPV-based organic solar cells - as a hole-selective contact [8], and also it has been entered into in light emitting diodes [9].

Despite importance of applications of γ-CuI [10-11], many scientific questions remain open. One of them is the nature of chemical bonding in γ-CuI. In the chemical stability aspect it is not clear, however, how the strong 5p(I)-3d(Cu) hybridization [12-14] is balanced with the other actual chemical interactions in the material. Our analysis showed that the existing ionic-covalent picture of chemical bonding treated in terms of nearest-neighbor bonds appears to be strongly inconsistent

with the (many-body) description of material properties. There are two reasons for this. The first is that the interatomic Cu-I distance of 2.62 Å is greatly shorter than the corresponding ionic bond length of 3.12 Å (evaluated as the sum of the Cu(I) and I(I) Pauling ionic radii). Moreover, this distance is smaller than the sum of the empirical covalent radii of the neighboring atoms (2.71 Å). Obviously, such specific length shortening reflects a structural peculiarity caused both by the strong intermixing and greater electron donations within Cu-I covalent interactions. The second reason relates to the size of electronic localization effects associated with Cu 3d valence electrons. In contrast to the case of cuprous oxide [15-16], most previous studies never gave the special quantum-mechanical consideration to the role of these effects. However, in the context of Cu-Cu and Cu-I bonding interactions, our preliminary analysis indicated that the distribution of Cu 3d valence electrons is enormously important both for the system integrity of chemical interactions in the material. This allowed us to suggest the advanced model that, in a large extent, recast the previous one by introducing the combination of metallic and covalent bonding patterns as the main origin of chemical bonding in γ-CuI. Moreover, in the present work we investigated the particular role of the 3d electron correlation effects in the system by means of the self-consistent GW approach. This in turn allowed us to perform the deep reexamination of the electron structure of γ-CuI.

We also note that the applicability potential of a semiconducting material as a working element of electronic and optoelectronic devices is essentially determined by specific requirements. Clearly, these requirements depend on a broad range of fundamental and processing factors. Increased interest in γ-CuI applications stimulated our theoretical studies in this field. The main goal of the present work was to perform a systematic analysis of the crystalline design of the bulk γ-CuI in such a way that could shed light on how the changes at the atomic level (i.e. changes in microstructure originating from the physicochemical treatment) lead to differences in the electronic

properties. Furthermore, a crucial aspect in the microstructure engineering of the synthesizable γ-CuI is the firm knowledge of the ground state properties of the material. Thus, we focused our research on the following main issues: First, we identified and assessed realistic "structure-property" connections that link the compositional and structural details to the electronic properties of γ-CuI. Secondly, because the structural stability of the solid CuI admits deviations from the idealized metal and halogen 1:1 stoichiometry, we analyzed how structural point defects may be governed by variations of the chemical content.

2. MATERIALS AND METHODS

2.1 Choice of the material

Research on cuprous iodide CuI has been widely covered in the literature over the past several decades (see, e.g., review articles in Refs. [17-20]). CuI belongs to a cuprous halide family Cu*X*; it is characterized by the monovalent copper(I) state which is stabilized by tetrahedral coordination to the surrounded four halogen atoms. In the crystalline state, under ambient conditions the solid CuI has a zinc-blend structure with the space group $F\bar{4}3m$. On heating, its face-centered cubic lattice suffers a sequence of two phase transformations, γ-CuI → β-CuI → α-CuI, characterized by transition temperatures 369°C and 407°C, respectively. Both of these polymorphs have very different crystal structures: β-CuI crystallizes in the hexagonal wurtzite structure (P63mc), while α-CuI - returns to the cubic rocksalt structure ($Fm\bar{3}m$).

2.2 Computational methods and details

Our calculations were performed within the framework of density functional theory (DFT) and Hedin's approximation in the GW method [21] by using the projector-augmented wave (PAW) pseudopotentials [22-24], as implemented in Vienna ab initio simulation package (VASP) [25]. The Kohn-Sham single-particle eigenstates were determined by using the Perdew-Burke-Ernzerhof (PBE) GGA exchange-correlation functional [26]. The electronic structure of γ-CuI was determined within the many-electron perturbation theory by means of the frequency-dependent quasiparticle GW approach [21]. The supercell of 63 atoms was used to simulate copper vacancies as single point defects in the lattice of γ-CuI. A series of convergence tests with respect to the plane-wave cutoff energy showed that the value of 600 eV provides well-converged free-energy results with the required degree of accuracy being below 1 meV. Periodic calculations have been employed with a Γ-point centered automatic mesh for the k-point sampling to perform Brillouin zone integrations. Tetrahedron method with the Blöchl corrections was applied for the integrations, for which 84 irreducible k-points for PBE-GGA, 112 for PBE-GGA supercell, 35 for HSE06, and 125 for GW calculations were used, respectively, to calculate the electronic structure. Equilibrium structural geometries were completely relaxed in PBE-GGA with respect to lattice constant and internal atomic positions. Optimized lattice parameter of 6.0578 Å is in a good agreement with the experimental value of 6.054 Å.

As relativistic effects may be important in heavy-element structural chemistry and physics (see, e.g., Refs. [27,28]), according to Ref. [29] we note that our periodic self-consistent calculations of the system of valence electrons in the solid γ-CuI are definitely scalar-relativistic. This in turn ensures that the relativistic corrections to the filled-$3d^{10}$ copper bands [30] are necessarily taken into

consideration. Moreover, scalar relativistic corrections are also included (via the use of scalar-relativistic orbitals) in the corresponding GW numerical procedures.

Additionally, the ground state of the system was analyzed in the scheme of Dudarev et al [31] by means of PBE+*U* calculations. The effective *d*-*d* Coulomb repulsion on the Cu site, Ueff = U-J, represented in terms of the difference of the Hubbard (U) and exchange (J) energies, was evaluated from the constrained PBE-GGA computations based on the linear response theory [32]. We obtained U_{eff}=0.5 eV. We decided to omit the results of GGA+*U* calculations because we found that because of the small value of *U* they do not vary from those of the corresponding PBE-GGA one-particle picture.

We note that the implementation of the practical computational scheme for the GW method in VASP is based on Hedin's approximation: the frequency-dependent self-energy Σ is expressed through the direct product of the perturbed Green's function and the dynamically screened Coulomb interaction Σ = iGW. We compared the performance of multi-shot series of the zeroth order in the self-energy G0W0, partially self-consistent GW0 and fully self-consistent GW numerical procedures with respect to materials parameters, such as experimentally determined values of the macroscopic dielectric constant ε_∞ and the fundamental band gap. We found that a multiple update of the orbitals and eigenvalues corresponding to multi-shot self-consistent GW calculations with the number of iteration steps of 10 are needed to correctly reproduce these data in close agreement with experiment. Moreover, comparison of the results of GW0 and GW approximations to Σ indicated that full accounting for the many- body dynamical effects is of prime importance in the electron structure calculations. In this context, we note that the smallness of the Hubbard energy (U_{eff}=0.5 eV) for the completely filled 3d states of Cu may also be indicative of the strong screening effects in the electron subsystem of γ-CuI.

To investigate how nonlocality contributes into the correction of the self-interaction error we investigated the electronic structure by means of the range-separated hybrid functional HSE06 [33-36]. Within hybrid functional formalism we adopted a strategy in which the amount of the exchange contribution is modeled by a material-dependent parameter - the inverse electronic dielectric constant [37-38]. Using macroscopic dielectric constant, estimated from the numerical procedures of GW methods, ε_∞=5.1, the relevant fraction of the Fock exchange in the HSE06 functional was modified to 0.196. The fundamental band gap of γ-CuI obtained from different approximations was evaluated to 1.13 eV within PBE-GGA, 2.30 eV within the modified HSE06, and 2.70 eV within the self-consistent GW approximation, respectively. It was therefore found that the GW approach accounting for quasiparticle corrections for the self-energy provides better agreement with experimentally established band gap value. It was chosen as the most suitable method for investigation of the electron structure of γ-CuI.

The role of non-locality can also be seen through testing of thermodynamic stability of γ-CuI in terms of the heat formation (ΔH_f^0). Our result of ΔH_f^0=-47.1 kJ/mol obtained by PBE-GGA calculations fairly agrees with those of Ref. [39] -30.9 kJ/mol and -62.5 kJ/mol obtained within PBE-GGA and GGA+*U*, respectively. Our result of ΔH_f^0= -77.7 kJ/mol within HSE06 agrees well with the experimentally established -67.8 kJ/mol [40] that indicates to importance of nonlocal effects in theoretical evaluation of the heat of formation of the solid γ-CuI.

The formation energy of a neutral Cu vacancy was evaluated using the formalism of the work [41]. In order to reduce spurious defect-defect interactions, finite-size error reduction method described in Ref. [42] was taken into account. Note that this enabled us to avoid the difficulties in theoretical estimates (based on the supercell approach) of the defect formation energy for the stable crystalline system that possesses the strong many-body dynamical corrections. Our PBE-GGA

estimate of 0.53 eV obtained within the formalism of [41,42] can be compared to the previous result of the work [39], 0.50 eV, calculated by using the GGA+U approach.

Post-processing procedures such as a grid-based Bader analysis [43-44] and the electron localization function (ELF) [45] were combined to investigate topological features of the valence electron distributions on the base of theoretical charge densities. Group-subgroup analysis and compilation sequences of the Bärnighausen tree [46] were conducted by means of the programs [47] hosted by Bilbao Crystallographic Server [48-50]. The ISOTROPY Software Suite [51] and the VESTA program [52] have been used in the course of evaluation of the crystal structures and electron topologies.

3. RESULTS AND DISCUSSION

3.1 Setup of theoretical modeling of γ-CuI assembly

We model an assembly of the equilibrium lattice geometry of periodic γ-CuI at the atomistic level by using an appropriate combination of group-theoretic analysis and results of the relevant DFT calculations. The assembly begins with the preparation of initial crystalline superstructure as a starting trial template. In the context of crystal chemistry, one common rule of crystal design is that the assembly should be constructive. In particular, it is important that the full space symmetry of the chosen template would conform to a maximal set of packing configurations [53]. Our situation satisfies such design requirements. Moreover, since the template presents enough freedom in choosing different configurational constraints, the crystal design of the solid γ-CuI may be characterized in terms of a distribution of iodine atoms. We note further that identical $\bar{4}3m$ point symmetry of 4*a* and 4*c* lattice sites determines the dichotomous character of the cubic structure of γ-CuI. This implies that the lattice geometry viewed in terms two interpenetrating complementary

sublattices admits two alternative crystallographic descriptions [54-55]. With respect to the geometrical interpretation of Wyckoff positions both descriptions are exactly congruent because they are fully transferable to each other by simple exchange of the Cu and I atomic sites. In the presented modeling scheme, we use the $F\bar{4}3m$ lattice geometry in which zero Wyckoff coordinates (0,0,0) are assigned to copper atoms, and (1/4,1/4,1/4) positions relate to iodine atoms. Such representation is very useful for configuring the copper sublattice as a scalable template capable to distribute iodine atoms. This in turn allows us to choose the assembly route of γ-CuI such that it may proceed through an extension of copper lattice with subsequent screening of the possible Cu-I coordinations, thus providing the proper formation of Cu-I bonds in the model. Also we employ the concept of an isotropy subgroup [56] which aids us in prediction of intermediate and final geometries.

3.2 Genesis of γ-CuI structure as a copper-driven assembly

The experimental synthesis of anhydrous cuprous iodide from the starting mixture of the elements is determined by the following reaction [57-58]:

$$\mathrm{Cu} + \mathrm{I} \rightarrow \mathrm{CuI}. \qquad (1)$$

If one renders synthesis route (1) in terms of the principal building blocks such as Cu and I atoms, one can model the formation of γ-CuI as a structural assembly that proceeds via packing and coordination of iodine atoms implemented into the host copper lattice. Figure 1 can be regarded as a copper-driven assembly scheme. Key to the design is that a global symmetry of the configuration space determined by the $Fm\bar{3}m$ space group presents vacant crystallographic voids to accommodate the iodine (guest) atoms. Figure 2 can be regarded as the relevant theoretical sketch of reaction (1) that describes the simulation of iodination of the *fcc* copper lattice, solved in terms of the

macroscopic transformation $Fm\bar{3}m \rightarrow F\bar{4}3m$. In Fig. 2A, the corresponding group-subgroup relation is written as the Bärnighausen tree [46]. Its important feature is that by connecting two targeted cubic structures it provides the required invariance of the starting 4*a* Cu positions with respect to the group-subgroup relation $Fm\bar{3}m \rightarrow F\bar{4}3m$ of index 2. Most favorable configuration of the iodine atoms was found from DFT based computational optimizations. The result is that the optimal binding between the Cu and I atoms entirely locates the iodine atoms into the preferential 4*c tet* positions. This is in a strict compliance with experiment [55] and group-theoretical predictions on the splitting of Wyckoff positions [59].

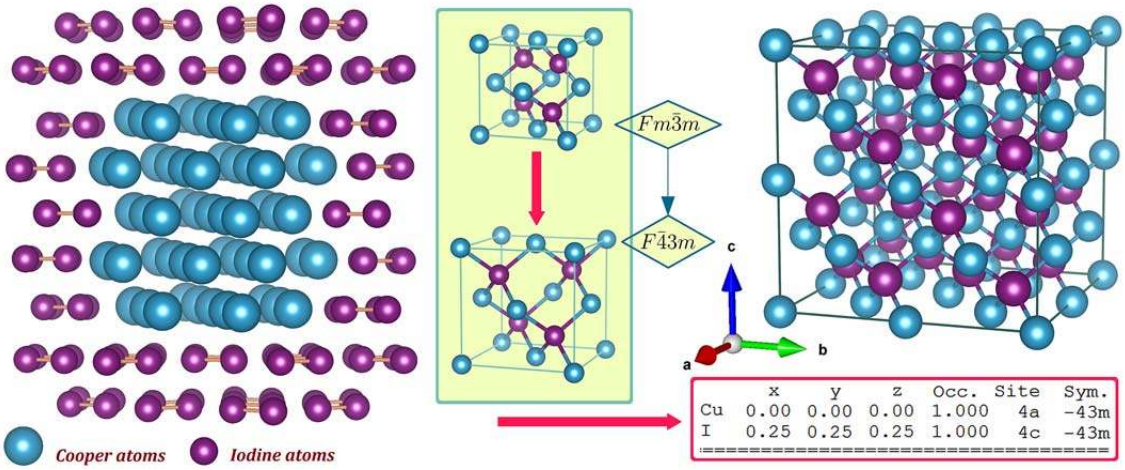

Figure 1. *Flowchart illustrating a copper-driven assembly of γ-CuI in the Cu-I system. Metallic copper represents a crystalline bulk template in which the packing of iodine atoms proceeds through the filling of interstices. Structural relationship between the template and the final phase is determined by the group-subgroup relation* $Fm\bar{3}m \rightarrow F\bar{4}3m$.

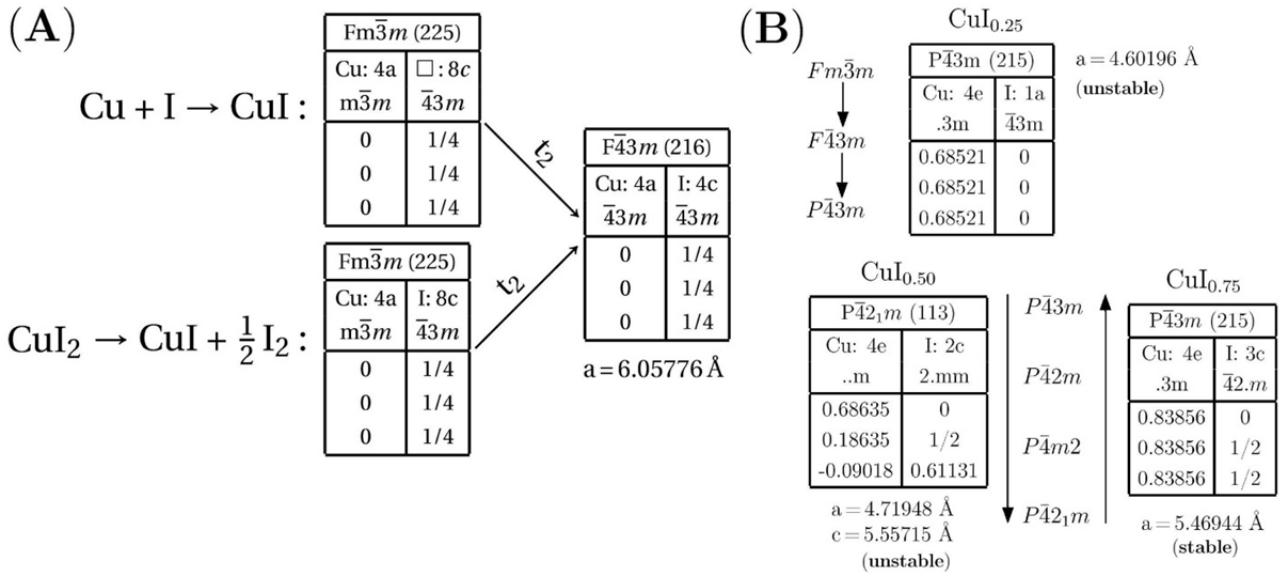

Figure 2. *Structural chemistry of the CuI assembly represented in terms of the Bärnighausen tree.* ***(A)*** *Schematic diagram of the formation of γ-CuI along the one-step* $Fm\bar{3}m \rightarrow F\bar{4}3m$ *pathway. Here the* $F\bar{4}3m$ *group is a t-subgroup of order 2 of* $Fm\bar{3}m$*. For convenience, we use the basis in which the Cu atoms occupy the 4a sites at (0, 0, 0) positions. Fcc bulk copper represented as* $Cu\square_2$ *is viewed as an idealized version of aristotype of the* CaF_2 *type. Symbol* □ *indicates the empty (vacant) tetrahedral interstitial position. Composition reaction* Cu + I → CuI *furnishes iodine atoms into the Cu lattice to fill the half of equivalent tetrahedral voids of the fcc structure. Partial decomposition reaction* $CuI_2 \rightarrow CuI + ½I_2$ *is associated with the effective cutting down of the number of occupied tetrahedral voids by one half; the I atoms are leaving these positions to form the molecular iodine. In both cases, the local symmetry of 4a crystallographic sites occupied by cooper atoms are preserved, but there occurs the reduction of the multiplicity of the Wyckoff positions related to the I atoms from 8 to 4.* ***(B)*** *Three intermediate stages of iodination of the copper lattice along with the predicted structural geometries. The iodination process is represented by the sequence of transformations which is described in terms of three hypothetical structures. These structures depend on the iodine content via the stoichiometry ratios of 1/4, 1/2, and 3/4, respectively. The first two structures, denoted as* $CuI_{0.25}$ *and* $CuI_{0.50}$*, are unstable, the third one with the composition of* $CuI_{0.75}$ *corresponds to the stable crystalline phase. The stability conditions were tested by using a vibrational analysis of imaginary modes in the zero point combined with checking elastic constants and relations between them.*

3.3 CuI *vs* CuI_2: why synthesis ends by formation of γ-CuI

One of advantages of the suggested assembly scheme is that it can explain the structural instability of the solid CuI_2 in terms of Cu(II) to Cu(I) reduction. The idea is to construct the trial 3D lattice template of a cubic symmetry conditioned by the following two constraints. First, we retain the initial global symmetry of the model system consistent with the $Fm\bar{3}m$ space group. This choice is necessary to create a composition route of CuI_2 as well as to secure the four-coordinate tetrahedral geometry of γ-CuI arising after decomposition. Secondly, we require that the point-site symmetry of all the Cu sites be preserved by the space symmetry of *fcc* lattice, while all the tetrahedral voids be filled by I atoms (as determined by the structural chemistry of the hypothetical CuI_2). The computational relaxations of the trial structure generated the fluorite crystalline architecture with the lattice constant of 7.148 Å; it is characterized by the doubled tetrahedral sites to which every Cu(II) is coordinated (as displayed in Fig. 2A). Our subsequent DFT examinations of structural and thermodynamical instabilities showed that such predicted fluorite geometry of CuI_2 does not exist under normal conditions because it is highly unstable. It was further examined that the loss in stability causes the decomposition of copper(II) iodide into copper(I) iodide and molecular iodine along the route $CuI_2 \rightarrow CuI + ½I_2$. As shown in Fig. 2A, removal of one of the two tetrahedral sites occupied by I corresponds to the pathway of decomposition of CuI_2 that arises within the cubic crystalline environment by means of the transformation [fluorite-structured CuI_2] → [zinc-blende CuI]. In light of the crystal chemistry the main reason why the loss in stability cannot be neutralized by formation of additional bonds is associated with the absence of the octahedral coordination which is typical characteristic of Cu(II) ion. We attribute this to the strong p-d hybridization which the system arranges in order to prevent the tetrahedral coordination from the reconstruction into the octahedral one. Correspondingly, the benefit of consideration of such particularly unstable geometry

of CuI_2 is that we gain a clear structural understanding of why synthesis reaction (1) prefers to form entirely the CuI phase and not CuI_2.

3.4 Activation of covalent bonds outward of metallic bonding

We will consider the qualitative model first. The electronic configuration of the outermost orbitals for copper $[Ar]3d^{10}4s^1$ and for iodine $[Kr]4d^{10}5s^25p^5$ assumes that since both elements are bonded together to form the binary CuI, they manifests the closed-shell *d* and *p* configurations, respectively. At first glance, such simple model of the direct metal-nonmetal bonding based on the $4s(Cu)\rightarrow 5p(I)$ charge transfer is self-explanatory. However, to get the whole picture, it is necessary to clarify the role of covalent and noncovalent effects.

Thus, our task is to describe the genesis of chemical bonding in γ-CuI in more detail. The important point of the γ-CuI assembly is that the four-coordinated (28-electron) copper cores form the host *fcc* lattice, which, as explained above, determines the ordered distribution of the guest iodine atoms upon half of empty interstitial cubic tetrahedral sites. Another important point - no octahedral coordination geometry associated with the Cu(II) charge state occurs. We note further that our DFT studies showed that the principal key to understanding the architecture of interatomic interactions is the transition from the metallic state of Cu to the insulating one of CuI. The main event here is the reformation of an energy landscape to account for new dependencies caused by incorporation of sufficient amounts of iodine and, correspondingly, to find a new global minimum. Figure 2B reflects in terms of the Bärnighausen tree a theoretical modeling of how iodination of the copper lattice proceeds according to reaction (1). The simulation of the synthesis is represented by three (hypothetical) intermediate stages which are characterized by the different amounts of the

incorporated iodine. All three stages we specify in Fig. 2B can be considered as indicative reference points on the transformation path from the metal to a binary compound of the ideal stoichiometry. The first two reference points are related to fully unstable crystalline structures of the iodine deficient $CuI_{0.25}$ and $CuI_{0.50}$ compounds. The structural stability of the composition of $CuI_{0.75}$ gives us an approximate estimate of the relevant end point of instability. In the rough, one can predict that reaction (1) may proceed in the bulk if the stoichiometry necessarily exceeds the 1/2 ratio.

A further comparison of the structural phases of Fig. 2B indicates that there is a direct correlation between three characteristic factors: the embedded (reacted) iodine amount, the favorable lattice positions preferred by I atoms for occupation, and the space symmetries of the equilibrium structure. In other words, the reference points appear to be useful descriptors for unraveling how the coordination environment effect guides the iodination process. For instance, in the case of small iodine content (represented by the first reference point $CuI_{0.25}$) the iodination process tests the $F\bar{4}3m$ structure native to the stoichiometric composition of CuI but finally prefers the $P\bar{4}3m$ cubic structure of slightly lower symmetry. A significant symmetry lowering to the tetragonal phase of the lattice geometry takes place for the second reference point $CuI_{0.50}$ characterized by the low-symmetry $P\bar{4}21m$ structure. It is achieved when the iodine content comes to half of Cu atoms. Stronger iodination recovers the $P\bar{4}3m$ cubic structure back and makes the crystalline phase of $CuI_{0.75}$ stable (the third reference point of $CuI_{0.75}$). Clearly, compared with the ideal stoichiometric composition of CuI, this stability is relative because the further iodination completes the stabilization in the form of the preferred $F\bar{4}3m$ structure (Fig. 2A).

Figure 3 represents reaction (1) from the structural chemistry point of view, i.e. all the three intermediate crystalline geometries which we have chosen as the specific reference points with respect to variable iodine content are displayed in terms of building blocks. Interestingly, the

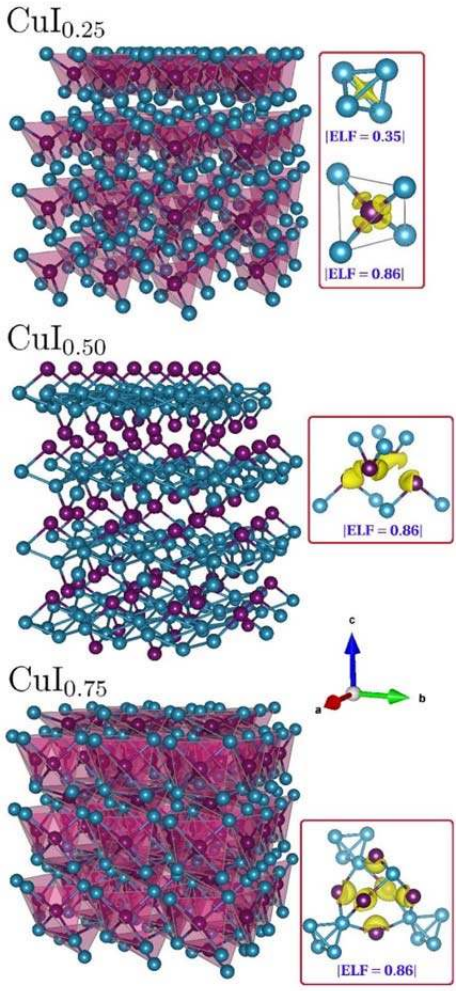

Figure 3. *Structural chemistry of the CuI assembly represented in terms of three intermediate phases of variable iodine content. The iodine content corresponds to the following stoichiometry (metal-to-nonmetal) ratios: 1/4, 1/2, and 3/4. The sequence of transformations and packing motifs were predicted on the base of DFT calculations The color codes are the same as in Fig. 2. The symmetry of the crystal structures is described in Fig. 1. In the iodine-deficient region represented by the composition of $CuI_{0.25}$, the geometry is based on the layers of perfect ICu_4 tetrahedrons whose stacking along the c axis is provided by Cu_4 trigonal pyramids. The next composition of $CuI_{0.50}$ corresponds to the tetragonally distorted cubic structure that consists of the layers composed of ICu_2 linear chains and bridged together through the network of Cu atoms. The solid-state structure of the composition of $CuI_{0.75}$ is formed as layers of strongly distorted corner-sharing ICu_4 tetrahedrons. The layers join together via Cu-Cu metallic linkage. ICu_4 tetrahedra are shaded in light cherry red. The total charge partitioning schemes are given in terms of valence ELF isosurface on the right-hand side. The numerical values of ELF for which visualizations were calculated are displayed below. The lobelike isosurface (in yellow) shown far beyond the bonding planes corresponds to a lone pair domain.*

instability of the $CuI_{0.25}$ and $CuI_{0.50}$ phases might be associated with a molecular character of their assembly because their crystalline architecture is based either on the ICu_4 or ICu_2 covalently bonded building blocks linked along the c-axis via Cu-Cu metallic network. Although the strength of the metal linkage is insufficient to stabilize the first two crystal structures, the direct comparison of the relevant bonding patterns is of great interest. An analysis of spatial topology of valence electron density at the each stoichiometry ratio revealed that the formation of chemical bonding proceeds in a similar way for all of these intermediate structures. The first important point to emphasize here is that the covalent and metallic (multicenter) interactions compromising the bonding picture become spatially separated when the iodine atoms begin to fill the copper lattice. In other words, we observe here the unusual effect of chemical bonding - spatial separation of covalent and metallic interactions (discussed earlier for some inorganic compounds [60-61]). The term "spatial separation" refers to the situation when the overall chemical bonding benefits directly from a spatial division of different arrangements of the valence electron density. Secondly, even an arbitrarily small amount of the embedded electron-rich iodine atoms activates covalent binding with copper because the iodine atoms achieve a complete 5p valence shell due to near-free 4*s* electrons that are available from the metallic copper in advance. Hence, the effect of spatial separation of chemical interactions exists for the whole range of the iodine content up to the equiatomic composition. At the same time, we note that the ratio covalency/metallicity and, correspondingly, the relative stability of covalently bonded framework depends strongly on the iodine content. Thirdly, the establishment of chemical bonding during the iodination process is mainly determined by an arrangement of iodine 5*p* valence electrons. In view of this, different Cu-I coordinations are formed in the intermediate phases. For example, the $CuI_{0.50}$ phase shows that with increase of the iodine content the perfect tetrahedral symmetry of I-Cu interactions established in $CuI_{0.25}$ with the ideal bond angle of 109.47° is reduced

to the lower symmetry of Cu_2I units with the bond angle of 103.21°. The $CuI_{0.75}$ phase illustrates that the further iodination of $CuI_{0.50}$ recovers the tetrahedral symmetry of the structural building blocks but distorts their shape in the notably imperfect form. In addition to the electron pairs shared in the covalent I-Cu bonds, the two last phases demonstrate the existence of non-bonding *p*-type lone pairs which are well-localized around the iodine atoms.

Further analysis of the results of computational modeling showed that the most suitable arrangement of valence electrons occurs only in the ideal stoichiometric composition of γ-CuI. For this $F\bar{4}3m$ structure the chemical bonding situation is essentially simplified because the system has completely eliminated from the total electron density distribution such patterns as direct metallic connections, and the presence of non-bonding *p*-type lone pairs. Note that the copper sublattice, which at the stoichiometry ratio contributed all the collectivized 4*s* electrons to the formation of the iodine 5p closed shells, retained the $3d^{10}$ closed-shell orbitals practically unaffected. This implies that the former multicenter Cu-Cu interactions have been converted into the effective atomic interactions that are characterized by repulsion forces acting between nearest copper sites. By analogy with the results of Refs. [62-63] such transformation allows us to regard these forces as specific (electrostatic) bonding pattern of the noncovalent nature.

Note also that the large value of the Cu^I-Cu^I miminal distance in a crystal-packing configuration of the solid CuI (4.28 Å) marginalizes the possible role of quantum dispersion forces between the metal centers [64]. In other words, analyzing the bonding in the material, we find no evidence to expect that in the crystal structure of γ-CuI copper atoms may interact in a metallophilic fashion. However, it would be reasonable to suggest that the artificial change of the native packing configuration of copper and iodine atoms may induce closed-shell cuprophilic interactions. An example of such system designed on the base of CuI is considered in Ref. [65].

In addition, it is interesting to discuss yet another aspect concerning the possibility to utilize the structural design of the present work in order to analyze the possible similarities between the bonding features of γ-CuI and noble-metal oxides Cu_2O, Ag_2O, and Au_2O [15-16]. In this context we note that all the cations of these oxides relate to simple metals Cu, Ag, and Au, respectively, which are crystallized in the same *fcc* geometry characterized by the $Fm\bar{3}m$ space group. Symmetry changes that accompany the relevant oxidation process are described in terms of group-subgroup relation $Fm\bar{3}m \rightarrow Pn\bar{3}m$ of index 4. The key feature of such structural transformation "host metal -> oxide" is that the crystallographic positions of the copper sublattice are practically unaffected, albeit the point symmetry slightly lowers from O_h to T_h. Similarly to the case of γ-CuI this indicates that no matter how the copper atoms bind chemically diverse ligands of the anionic sublattice they retain the general pattern of the former metallic interactions through its reconstruction into the new ordering pattern of noncovalent interactions. In fact, this finding may be regarded as providing evidence from the structural chemistry on the existence of specific coupling in the copper sublattice of the noble-metal oxides. Thereby, regardless of oxidation scheme, analysis of the assembly modeling of the oxides may give a further confirmation of previous studies on the features of chemical bonding picture.

3.5 Character of elastic properties as a measure of chemical interactions

Compared with the Cu-Cu distance of 2.57 Å in *fcc* Cu, the electrostatic repulsion between nearest copper atoms lengthens this distance to 4.28 Å in γ-CuI. In Table 1, it is indicated how the expansion of the cell volume caused by the transformation Cu → CuI changes macroscopic elastic properties of the system. One can observe a sharp drop in all the elastic constants and characteristics

as compared with *fcc* Cu. In structural aspect, albeit the necessary stability conditions $C_{11}>0$, $C_{44}>0$, and $C_{11}-C_{12} > 0$ are satisfied, this implies that the γ-CuI lattice geometry is strongly soften once iodine is fully accommodated in the system. Indeed, as it is seen from the smallness of constants C_{44} and G^*, the γ-CuI structure is characterized by the small resistance of against a shear.

Table I. Independent components of the elasticity tensor C, the bulk modulus B, and the shear modulus $G^* = (C_{11} - C_{12})/2$ *for [110] shears in comparison with experimental data for fcc Cu. The values of the elastic constants were evaluated for γ-CuI within PBE-GGA. Previous results of theoretical calculations along with experimental data are summarized in Ref. [66].*

	C_{11} (GPa)	**C_{12}** (GPa)	**C_{44}** (GPa)	**B** (GPa)	**G^*** (GPa)	**C_{12}/C_{44}**
γ-CuI	54	35	22	41	9	1.6
fcc Cu Ref. *[67]*	170	122	76	138	24	1.6

In crystal chemistry aspect, because of the large difference between B and G^* values ($B >> G^*$) such global lowering in the elastic properties (in comparison with fcc Cu) can be rationalized via softening the Cu-Cu central connections, which is more energetically favorable than a variation of a length of the strong Cu-I covalent bond. At the same time, the anisotropy parameter represented by the ratio C_{12}/C_{44} does not noticeably change upon iodine incorporation. This important result indicates, that the role of the Cu-Cu central connections inherits by default as the property of the host fcc Cu lattice, and thereby remains a fundamental part of the total chemical bonding in γ-CuI, regardless of the fact that iodine incorporation increased the spacing between neighboring copper atoms. Of course, because of the large Cu-Cu spacing the strong covalency between two sublattice of γ-CuI is additionally needed in order to provide the global stability of the crystal lattice.

3.6 Electron structure of γ-CuI governed by covalent bonding

Note that one of the starting points of the present theoretical design is that the metallic copper considered as a reference system and γ-CuI are closely related with respect to structural assembly and stabilization. Previous studies have shown that in metallic copper the completely filled $3d^{10}$ shells are characterized by a weak interatomic interaction, a conduction band is formed by the outermost 4*s* orbitals from each atom, and Fermi surface is a nearly isotropic [68-69]. In view of these facts one can predict, in a qualitative sense, two main factors responsible for genesis of the electron structure of γ-CuI. First, since the local crystal environment (relating to the Cu atoms) changes considerable little at the transformation to the γ-CuI geometry (Fig. 2A), we may suggest that just nearly free s electrons are captured by iodine atoms when they are distributed in the copper sublattice. Secondly, as the electron collectivization is the macroscopic effect, we may suggest that the chemical confinement of the copper 4*s* electrons with iodine atoms is realized in the form of the directional metal-ligand binding (*pd*-type hybridization), thus dispelling a delocalized bonding as typical in *fcc* Cu and providing a stabilization of the iodine atoms in the separate sublattice.

Table II. Charge characteristics of atoms in γ-CuI as compared with other structural variants of the iodine-deficient Cu-I system (in units of |e|). The Pauling electronegativity values, f_P, are taken from Ref. [70]. Formal charges q_{ion} are determined by the closed-shell configurations. The quantities Q_B denote the Bader effective charges calculated from valence electron densities.

	f_P	q_{ion}	Q_B	Q_B	Q_B	Q_B
			γ-CuI	$CuI_{0.25}$	$CuI_{0.50}$	$CuI_{0.75}$
Cu	1.90	+1	+0.31	+0.056	+0.10	+0.21
I	2.66	-1	-0.31	-0.22	-0.20	-0.28

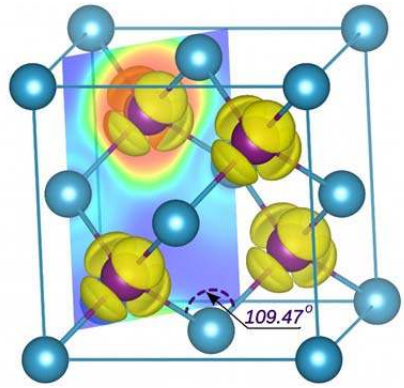

Figure 4. *Visualization of the valence electron density of CuI pictorially represented by the ELF isosurface at ELF=0.86. The covalent bonding is associated with the regions of localized electron pairs. The shift of the electron clouds towards iodine reflects the polar character of the shared electron connections. 109.47 ° is the bond angle in a tetrahedral environment.*

Post-processing analysis of the relevant valence electron partitioning schemes confirms these qualitative predictions; the results of analysis, which are summarized in terms of descriptors in Table 2, and depicted in Figure 4 in terms of the ELF isosurfaces, allowed us to quantify structure-bonding-properties. Comparison of the effective charges of Table 2 indicates that regardless of the electronegativity difference with respect to iodine, Cu demonstrates the low oxidation state of about +0.31. This is the direct evidence of well-developed covalency in the system. The next confirmation comes from Fig. 4 which in the spatial region of the central Cu shows a dense distribution (high ELF values) of the valence electron density pushed toward the adjacent I atoms. In view of small values of the Bader charges (as compared with nominal ionic charges), such area where shared electrons are distributed with a higher probability corresponds to the formation of the directional covalent connections of *pd*-type along the tetrahedral directions. As outlined in Fig. 4 the geometry of shared electron pairs is characterized by the bond angle of 109.47°. Therefore, in line with previous studies we are dealing with the strong *pd*-hybridization which according to the classification of the present work represents another main contribution to the total chemical bonding in γ-CuI.

To obtain the electron structure of γ-CuI we moved beyond the standard DFT approach. Figure 5 presents total density of states (TDOS) as well as orbital and site projected DOS (PDOS), respectively, calculated in the self-consistent GW approach. According to the suggested bonding scheme a tight binding of the 4*s* copper electrons with iodine atoms leads to the repulsion of the relevant bonding and antibonding states, which is accompanied by appearance of the insulating band gap. Due to separation of the copper and iodine valence shells the gap opens at the Γ point of the electronic spectrum. Electron sharing between the 3*d* Cu and 5*p* I orbitals contributes both to the top of the valence band and to lower energy states, thus forming the subband of about 2 eV width composed of the strongly hybridized Cu 3*d* and I 5*p* states. Indeed, the hybridization governs also the effect of the e_g-t_{2g} mixing of the relevant Cu 3*d* orbitals in this subband. Compared to previous

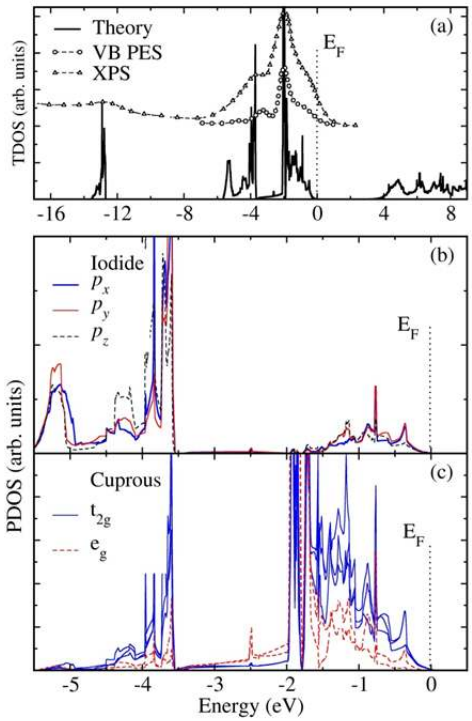

Figure 5. ***(a)*** *TDOS calculated for CuI within the self-consistent GW approach as compared to results of valence band photoemission spectroscopic (VB PES) [61] and X-ray photoelectron spectroscopic (XPS) [14] studies.* ***(b)*** *and* ***(c)*** *PDOS for p states of iodine and d states of Cu, respectively. Fermi level is set to zero eV.*

theoretical studies of the electron structure, we emphasize that our self-consistent GW calculations are in reasonably good agreement with experimental data *[14, 71]* as well as that dynamical correlation effects essentially enhance the overall valence electron localization, what suggests a significant role they are playing in binding energetics of the *p-d* hybridization channel.

The last step is to explain why the application of the self-consistent GW method is needed to obtain an accurate evaluation of the electron structure of γ-CuI. As seen from the numerical data presented in subsection 2.4, the band gap value is highly underestimated in the semilocal GGA-DFT calculations. From further numerical estimates it became clear that it is necessary to employ about 30% of the Fock exchange amount as a fitting parameter in the HSE06 hybrid density functional in order to minimize self-interaction effects and, correspondingly, to obtain the band gap comparable with experiment. On the other hand, application of the GW approach showed that the performance of both G_0W_0 and partially self-consistent GW_0 calculations is unsatisfactory as well. In contrast, the self-consistent GW calculations gave a reliable quasi-particle picture, although a slow convergence has been demonstrated.

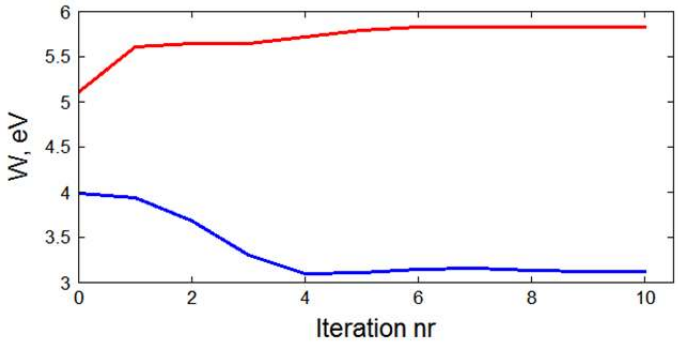

Figure 6. *Convergence of quasiparticle energies in the self-consistent GW calculations. The upper red line corresponds to the bottom of the conduction band; the lower blue line corresponds to the top of the valence band.*

On the theoretical side, it is important to highlight that in γ-CuI we are dealing with two complementary mechanisms of chemical coupling that are governed by the electron subsystem; we have shown they are spatially separated and operate in various ways with respect to the relevant binding sites. Accordingly, there arises a question what should be regarded responsible for the many-body dynamical correlations that are covered by the self-consistent GW calculations. As shown in Fig. 6, the effect of these correlations equally affects electrons residing at the valence and conduction band edge positions. Given the number of iterations of the GW procedure, one can conclude from these results that the quasi-particle energies of the electronic states relating both to the minimum of the conduction band and the maximum of the valence band appear weaker convergent. Taking into account that the largest part of the states of the valence band is formed of the copper 3d electrons mixed with the iodine 5*p* electrons, it becomes clear that just valence electrons of the 3d orbitals are primarily involved in the correlation effects. At the same time, the largest part of the GW lowest excited states are represented by 4s copper empty orbitals. We suggest that important in this case is the role of one-center metal 3*d* - 4*s* hybrid excitations. The most convincing argument for that can be taken from the Orgel model of d-orbital holes [72], i.e. in the context of the formal $3d^{10}$ electron configuration the higher 4s unoccupied orbitals may accommodate electrons to participate in the metal-metal bonding. Moreover, since the 3d - 4s charge transfer has the intra-atomic nature, the electronic correlations that are subject to the many-body dynamical effects should demonstrate the short-range behavior. On the base of results presented in Ref. [73], we can come to an understanding that just the slow convergence of the correlation energy causes the slow convergence of quasi-particle energies in the self-consistent GW calculations. Interesting evidence is that, in such complex situation neither G_0W_0 nor GW_0 approximations do not even work well as would suppose because the dynamically screened Coulomb interaction W

substantially better mediates the short-range (on-site) electron-electron interactions than the bare one W_0. Furthermore, it seems reasonable to conjecture that we are dealing in the electron subsystem of γ-CuI with the specific effect of many-body localization occurring within the manifold of the copper 3*d* valence electrons. This effect may be the leading reason why in calculations the change of the theoretical band gap is so responsive to full cancellation of the self-interaction error. In fact, in the context of copper bonding the 3*d*-4*s* delocalization channel does not correlate with the covalent interactions established with the iodine atoms (as it is seen from the above analysis of iodination processes). As a result, for keeping the electron stability the system increases the band gap to reduce the valence charge delocalization in the copper sublattice.

3.7 Testing of optical responses of γ-CuI

Based on the self-consistent GW approach, we next discuss the optical responses of the material in terms of the energies of the single quasi-particle states. Figure 7A shows the results of theoretical

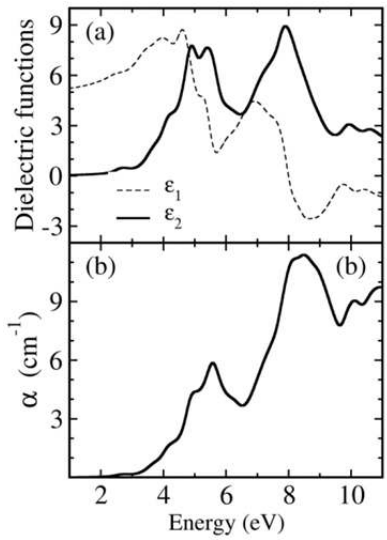

Figure 7. *Many-body simulation of optical responses of γ-CuI.* ***A.*** *Real and imaginary parts of the frequency-dependent dielectric function.* ***B.*** *Absorption spectra.*

calculations for the real and imaginary parts of the frequency-dependent dielectric function, and the model of absorption spectra with respect to the energy of incident electromagnetic radiation. Analysis shows that the material can be characterized well transparent to the visible light because the simulated spectra demonstrate three spectral regions of intense absorption belonging mainly to the UV region. Evidently, this behavior is due to representative features of valence electrons such as the closed shells of frontier 3d copper orbitals and lower-lying *p-d* hybridized states, as determined in Fig. 6. The calculated quasi-particle absorption spectrum of CuI (Fig. 7A) indicates the fundamental absorption edge in the region of about 2.7 eV. This result is in a good agreement with the experimental data which demonstrate that the material is a wide-band gap semiconductor. Next we note that the simulated transmission spectrum agrees also with experiment.

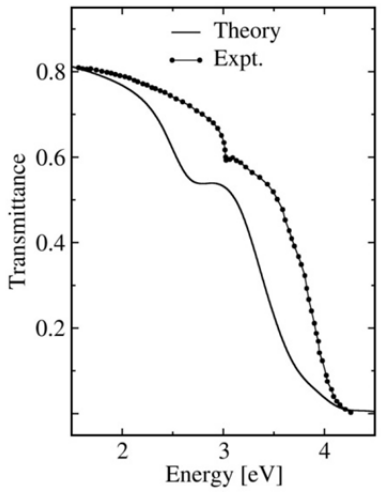

Figure 8. *Transmission spectra for γ-CuI calculated by self-consistent GW calculations in this work (—) as compared to that measured experimentally in Ref.[14] (●—●).*

In Fig. 8 we compared the results of our GW computational simulations with data of experimental observations. In fact, such comparison in the field of optics represents a good test for

the GW approach applied. It is seen that the measured curve appears to be similar to the simulated one. The certain difference is not surprise because of two possible reasons. The first one has theoretical character in the sense that the further account for the excitonic contributions which are actual in the absorption region may adjust the agreement with the experiment. The second reason is associated with the dependence of material properties on the routes of its preparation; this may definitely influence the optical spectra.

3.8 Cubic cuprous iodide as an intrinsic p-type semiconductor

From a crystal chemistry perspective, using the theoretical framework provided in the present work for the assembly scheme of γ-CuI, we can shed light on the possible classes of structural point defects. For example, whichever an experimental processing route one can prepare the γ-CuI samples of various sizes and shapes the occurrence of an excess amount of copper or iodine atoms in γ-CuI is highly unlikely. The corresponding explanation is based on an analysis of the terms and constrains which govern the distribution of iodine atoms in the host copper lattice. First, thanks to reaction (1), in the γ-CuI assembly, the starting precursors are so joined by chemical interactions that the most suitable occupation of the relevant crystallographic sites corresponds to the formation of a stoichiometric lattice. This implies that since the assembly design uses the fcc cubic packing of copper atoms as a crystalline template suggesting that such copper sublattice is internally preserved under the structural transformation, thereby it never chose any off-site Cu extra atoms as additional binding sites localized elsewhere in the system. Secondly, as to iodine atoms, computational simulations represented by Figs. 1 - 3 showed that the global stability requires that the iodine atoms be arranged just in the tetrahedral sites of the stoichiometric geometry to avoid

undue stresses and to minimize the total energy. Note that the intermediate positions other than tetrahedral sites are characterized by a higher energy. Therefore, theoretical modeling insights into structural features of γ-CuI allow us to suggest that the real synthesis conditions leave excessive amounts of both copper and iodine atoms no room for energetically favorable distributions other than those designated by the stoichiometric $F\bar{4}3m$ structure of γ-CuI.

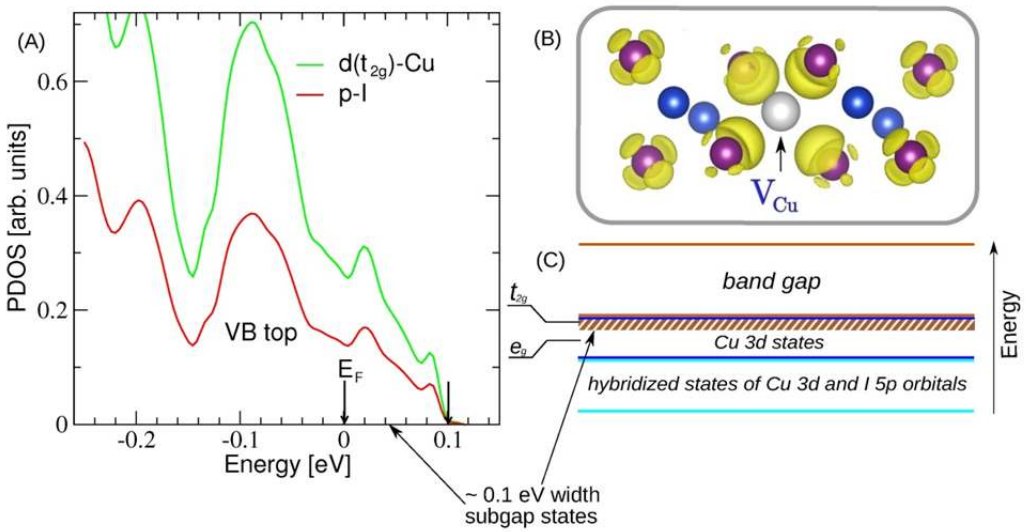

Figure 9. *The calculation results for the γ-CuI supercell containing a single copper vacancy (V_{Cu}). (A) PDOS represented in terms of Cu 3d and I 5p orbitals for the energy region close to the Fermi level. The first arrow labels the Fermi energy E_F, the second one indicates the total width of the empty subgap states. (B) An ELF visualization of the valence electron density represented by the isosurface at ELF=0.86. The picture displays a local region with the V_{Cu} defect-related void. The color legend is the same as in Fig. 1 (C). Sketch of the simplified energy diagram that outlines the electron structure of γ-CuI.*

Thus, all the above considerations direct us to the basic point of view that copper and iodine vacancies may be the most probable native defects in γ-CuI. In this work, we performed qualitative examination of the single copper vacancies V_{Cu}. For the sake of illustration, we assumed the presence of 3% of the neutral V_{Cu} (constitutional) defects. This corresponds to the partially

nonstoichiometric composition of the cubic $Cu_{1-\delta}I$ with small variance δ=0.03125. Shown in Fig. 9A in the energy range close to E_F is the relevant pattern of the calculated PDOS. It can be directly compared with that of Fig. 5 corresponding to the stoichiometric composition. It is seen that the effect is localized in the energy scale: the V_{Cu} vacancy creates shallow acceptor levels within the band gap located in the interval of 0.0-0.1 eV. As a result, these subgap electronic states generate the narrow-width band of the *p-d* hybridized holes. The corresponding tests of valence charge density redistribution showed that the appearance of the additional 3*d*-5*p* hybridization seems to have two fascinating factors associated with the neutral V_{Cu} vacancy. The first one, as indicated in Fig. 9B shows how the valence electron density is redistributed around V_{Cu}. The crucial point here is that the effect of redistribution that is associated with four nearby iodine atoms surrounding V_{Cu} is strong enough to provide a local extension of the *p-d* hybridization to the empty defect states. The second factor is that the variations of valence bond lengths and angles in the structure of the nearest neighbor iodine atoms around the relaxed V_{Cu} vacancy have minor character. This in turn ensures overall performance ability of the system with intrinsic defects because such amount of the introduced copper defects does not affect the main properties of the original electron structure. The obtained results allow us also to suggest a synergistic effect that makes possible the formation of defects favored just on the Cu sites. For example, the calculations showed that the formation energy of the copper vacancy V_{Cu} is characterized by low value of 0.53 eV.

We next show that useful application of our results provides the basis for the microscopic understanding why the crystalline γ-CuI as p-type semiconductor may demonstrate the desired characteristics of a TCO material. All we need to do is to deduce a simplified energy diagram on the basis of Figs. 5 and 9A. It is outlined in Fig. 9C. As we can see, the picture of the occupied and unoccupied bands can be represented by two contributions to the electron structure, one mainly from

3*d* Cu orbitals and the other - predominantly from the empty *s* orbitals at higher energies. Such scheme appears to be effectively sufficient to describe the principal features of the optical properties of γ-CuI for the visible range of the solar spectrum and, correspondingly, to obtain favorable agreement with experiment [Fig. 8]. On the other hand, the presence of empty sub-gap electronic states above the top of the valence band may give rise to a *p*-type conductivity. The key role here belongs to the additional *p*-*d* hybridization because by mixing iodine 5*p* and copper 3*d* states it secures hole mobility to be within an adequate range of values. This conclusion appears to be important in the technological aspect, i.e. to fit together both properties at the macroscopic level, the structure of γ-CuI should be tailored on the nanometer scale by providing the bulk material with copper vacancies. Moreover, the selective control of these vacancies during the synthesis of samples may allow one to develop the customized levels of *p*-type conductivity.

3. CONCLUSIONS

In this work, we have elaborated a most general theoretical scheme that provided the microscopic basis for realistic understanding of different properties of γ-CuI. By using the combination of DFT-based computational and group theory methods we have reproduced at the atomistic level the synthesis of the solid γ-CuI in terms of assemblies of crystalline geometries. Next, we showed that the developed systematic approach is of special importance to draw up the correct chemical bonding picture in γ-CuI. Feasibility of the approach is that the results of the computational simulations allowed us to distinguish the role of different chemical interactions in the overall bonding picture. Distinct from the earlier reports , the obtained results led us to the greatly improved scenario of chemical bonding in γ-CuI. It can be represented in terms of the composition

of covalent and noncovalent bonding patterns: strong covalency caused by *pd*-type reorganization of the electron orbitals, and repulsion of copper $3d^{10}$ closed-shell orbitals.

In the crystal design context, we have shown that the metallic copper lattice represents a bulk periodic superstructure that serves as an original template for distribution of iodine atoms. "Proofreading" generation of the native structure of γ-CuI proceeds via the distribution over favorable template positions that never match with the copper sites. Since packing of copper atoms keeps their initial arrangement fixed, the subsequent homogeneous lattice expansion of the template is caused by reorganization in electron densities of both participants. New charge distribution makes copper 4*s* free electrons tightly localized due to activation covalent Cu-I bonds with the "guest" atoms instead to allow them to maintain Cu-Cu metallic interactions. As a result, the covalent capture of iodine in the tetrahedral sites makes covalency in γ-CuI necessary structurally-specified with respect to both character of tetrahedrally coordinated hybridization and observed intrabond angles of 109.47°.

The presence of the strong covalency in γ-CuI, which is characterized by the maximization of the relevant electron states overlap, indicates that the realistic calculation of the target electron structure of γ-CuI much depends on how well the electronic correlations have been taken account in the theoretical scheme. We suggested that the presence of the electron sharing and closed-shell repulsion effects in the electron subsystem of γ-CuI may create a situation when many-body effects are *de facto* significant. In this aspect, our many-body reinvestigation of the γ-CuI electron structure by means of the GW method showed better and more realistic results on electronic and optical properties as compared with previous studies. Further application of our innovative approach allowed us to accurately model defect chemistry of γ-CuI in terms of copper vacancies. Among the

intrinsic point defects, the copper vacancies are found to be of great importance in light of an opportunity to govern the electronic and transport properties of the γ-CuI films.

ACKNOWLEDGMENT. NOTUR supercomputing facilities of Norway have been used in the computational work through the project nn4608k. S. K. gratefully acknowledges financial support from the Research Council of Norway through the New Indigo project 237643/E20, and support within internal project of the Institute for Energy Technology, Kjeller, Norway. The authors would like to thank Dr. M. Klopov for his attention to this work. SZK thanks Professor A. Subrahmanyam, Indian Institute of Technology Madras, Chennai, India for fruitful discussions related to the material that was under the focus of present research.

References

1 P. M. Sirimanne, T. Soga, and M. Kunst, J. Solid State Chem. **178**(10), 3010-3 (2005).

2 J. X. M. Zheng-Johansson, I. Ebbsjö, and R. L. McGreevy. Solid State Ionics **82**(3-4), 115-22 (1995).

3 J. X. M. Zheng-Johansson and R. L. McGreevy, Solid State Ionics **83**(1-2), 35-48 (1996).

4 S. Miyake, S. Hoshino, and T. Takenaka, J. Phys. Soc. Jpn. **7**(1), 19-24 (1952).

5 W. Bührer, W. Hälg, *Crystal structure of high-temperature cuprous iodide and cuprous bromide A2 - Armstrong, R.D.* International Symposium on solid ionic and ionic-electronic conductors: Pergamon; 701-4, (1977).

6 A. R. Zainun, M. H. Mamat, U. M. Noor, and M. Rusop, Mater. Sci. Eng. B. **17**(1), 012009 (2011).

7 G. A. Sepalage, S. Meyer, A. Pascoe, A. D. Scully, F. Huang, U. Bach, Y.-B. Cheng, and L. Spiccia, Adv. Func. Mater. **25**(35), 5650-61 (2015).

8 J. A. Christians, R. C. M. Fung, and P. V. Kamat, J. Am. Chem. Soc. **136**(2), 758-64 (2014).

9 S. A. Mohamed, J. Gasiorowski, K. Hingerl, D. R. T. Zahn, M. C. Scharber, S. S. A. Obayya, M. K. El-Mansy, N. S. Sariciftci, D. A. M. Egbe, and P. Stadler, Solar Energy Mater. Solar Cells **143**, 369-74 (2015).

10 D. Ahn and S.-H. Park, Sci. Rep. **6**, 20718 (2016).

11 N. Yamada, R. Ino, and Y. Ninomiya Chem. Mater. **28**(14), 4971-81 (2016).

12 P. Yu and M. Cardona, *Fundamentals of Semiconductors: Physics and Materials Properties*. 3rd Edition ed. Berlin And Heidelberg Gmbh & Co. Kg: Springer-Verlag; 2005.

13 M. Kobayashi, *Electronic structure of superionic conductors*. In: Takahashi TSaH, editor. Physics of Solid State Ionics. Fort P.O., Trivandrum-695 023, Kerala, India: Research Signpost; 1-15, (2006).

14 A. Goldmann, J. Tejeda, N. J. Shevchik, and M. Cardona, Phys. Rev. B **10**(10), 4388-402 (1974).

15 A. Filippetti and V. Fiorentini, Phys. Rev. B **72**(3), 035128 (2005).

16 P. A. Korzhavyi and B. Johansson, *Thermodynamic properties of copper compounds with oxygen and hydrogen from first principles*. SKB Technical Report TR-10-30, ISSN ISSN: 1404-0344, Stockholm: 28, (2010).

17 A. G. Massey, *27. - COPPER*. The Chemistry of Copper, Silver and Gold: Pergamon; 1-78, (1973).

18 A. Goldmann, Phys. Stat. Solidi (b) **81**(1), 9-47 (1977).

19 D. Chen, Y. Wang, Z. Lin, J. Huang, X. Chen, D. Pan, and F. Huang, Cryst. Growth Des. **10**(5), 2057-60 (2010).

20 B. Sharma and M. K. Rabinal, J. Alloys Compd. **556**, 198-202 (2013).

21 L. Hedin, Phys. Rev. **139**(3A), A796-A823 (1965).

22 P. E. Blochl, Phys. Rev. B **50**(24), 17953-79 (1994).

23 G. Kresse and D. Joubert, Phys. Rev. B **59**(3), 1758-75 (1999).

24 G. Kresse, J. Hafner, Phys. Rev. B **47**(1), 558-61 (1993).

25 G. Kresse and J. Furthmüller, Phys. Rev. B **54**(16), 11169-86 (1996).

26 J. P. Perdew, K. Burke, M. Ernzerhof, Phys. Rev. Lett. **77**(18), 3865-8 (1996).

27 P. Pyykko. *Chem. Rev.* **88**(3), (1988), 563-94.

28 P. Pyykkö. *Annu. Rev. Phys. Chem.* **63**(1), (2012), 45-64.

29 J. Hafner. *J. Comput. Chem.* **29**(13), (2008), 2044-78.

30 J. Hafner. *Quantum Theory of Structure: sp-Bonded Systems*. In: Hafner J, Hulliger F, Jensen WB, Majewski JA, Mathis K, Villars P, et al., editors. Cohesion and Structure: North-Holland; 147-286, (1989).

31 S. L. Dudarev, G. A. Botton, S. Y. Savrasov, C. J. Humphreys, and A. P. Sutton. Phys. Rev. B **57**(3), 1505-9 (1998).

32 M. Cococcioni, PhD. A LDA+U study of selected iron compounds Trieste: International School for Advanced Studies (SISSA), ; 2002.

33 A. Schleife, C. Rödl, F. Fuchs, J. Furthmüller, and F. Bechstedt, Phys. Rev. B **80**(3), 035112 (2009).

34 S. André, R. Claudia, F. Jürgen, and B. Friedhelm New J. Phys. **13**(8), 085012 (2011).

35 A. Schleife and F. Bechstedt, J. Mater. Res. **27**(17) 2180-9 (2012),.

36 G. Cappellini, J. Furthmüller, E. Cadelano, and F. Bechstedt, Phys. Rev. B **87**(7), 075203 (2013).

37 M. A. L. Marques, J. Vidal, M. J. T. Oliveira, L. Reining, and S. Botti, Phys. Rev. B **83**(3), 035119 (2011).

38 J. He and C. Franchini. Phys. Rev. B **86**(23), 235117 (2012).

39 H. Dan, Z. Yu-Jun, L. Shen, L. Chang-Sheng, N. Jian-Jun, C. Xin-Hua, Y. Chun-Mei. J. Phys. D: Appl. Phys. **45**(14), (2012), 145102.

40 D. R. Lide. *CRC Handbook of Chemistry and Physics, 83rd Edition*: CRC Press 2002.

41 S. B. Zhang, J. E. Northrup. Phys. Rev. Lett. **67**(17), (1991), 2339-42.

42 N. D. M. Hine, K. Frensch, W. M. C. Foulkes, M. W. Finnis. *Phys. Rev. B*. **79**(2), (2009), 024112.

43 E. Sanville, S. D. Kenny, R. Smith, and G. Henkelman, J. Comput. Chem. **28**(5), 899-908 (2007).

44 W. Tang, E. Sanville, and G. Henkelman, J. Phys.: Condens. Matter. **21**(8), 084204 (2009).

45 B. Silvi and A. Savin, Nature **371**(6499), 683-6 (1994).

46 H. Bärnighausen, MATCH Commun. Math. Chem. **9**, 139-75 (1980).

47 S. Ivantchev, E. Kroumova, G. Madariaga, J. M. Perez-Mato, and M. I. Aroyo, J. Appl. Crystallogr. **33**(4), 1190-1 (2000).

48 I. Aroyo Mois, M. Perez-Mato Juan, C. Capillas, E. Kroumova, S. Ivantchev, G. Madariaga, A. Kirov, and H. Wondratschek, Z. Kristallogr. **221**, 15 (2006).

49 M. I. Aroyo, A. Kirov, C. Capillas, J. M. Perez-Mato, and H. Wondratschek, Acta Crystallogr. A **62**(2), 115-28 (2006).

50 M. I. Aroyo, J. M. Perez-Mato, D. Orobengoa, E. Tasci, G. de la Flor, and A. Kirov. Bulg. Chem. Commun. **43**, 183 (2011).

51 H. T. Stokes, D. M. Hatch, and B. J. Campbell, ISOTROPY Software Suite, iso.byu.edu; H. T. Stokes and D. M. Hatch, J. Appl. Cryst. **38**, 237-238 (2005).

52 K. Momma and F. Izumi, J. Appl. Crystallogr. **44**(6), 1272-6 (2011).

53 A. Pishtshev and P. Rubin, Phys. Rev. B **93**(6), 064113 (2016).

54 M. A. Cooper and F. C. Hawthorne, The Canadian Mineralogist **35**(3), 785-6 (1997).

55 S. Hull and D. A. Keen, Phys. Rev. B **50**(9), 5868-85 (1994).

56 H. T. Stokes and D. M. Hatch. *Isotropy Subgroups of the 230 Crystallographic Space Groups* World Scientific, Singapore; 1988.

57 R. A. J. Shelton, Trans. Faraday Soc. **57**(0), 2113-8 (1961).

58 P. Senthil Kumar, Y. L. Saraswathi, and C. S. Sunandana, Mater.Phys.Mech. **4**, 71-5 (2001).

59 *Bilbao Crystallographic Server*. http://www.cryst.ehu.es/.

60 *General aspects of the spatial separation of chemical interactions were considered in [53] for materials $Mg_{11}Rh_{18}B_8$ and $Mg_3Rh_5B_3$ of the ternary Mg-Rh-B system*.

61 A. M. Alekseeva, A. M. Abakumov, A. Leither-Jasper, W. Schnelle, Y. Prots, G. V. Tendeloo, E. V. Antipov, and Y. Grin. Chem. Euro. J. **19**(52), 17860-70 (2013).

62 D. Bende, Y. Grin, and F. R. Wagner, Chem. Euro. J. **20**(31), 9702-8 (2014).

63 D. Bende, F. R. Wagner, Y. Grin, Inorg. Chem. **54**(8), 3970-8 (2015).

64 P. Pyykkö. *Chem. Rev.* **97**(3), (1997), 597-636.

65 N. Kuganathan, J. C. Green. *Chem. Commun.* (21), (2008), 2432-4.

66 F. El Haj Hassan, A. Zaoui, and W. Sekkal, Mater. Sci. Eng: B **87**(1), 40-7 (2001).

67 G. Simons and H. Wang. *Single crystal elastic constants and calculated aggregate properties.* . MA, USA: MIT Press, Cambridge; 1977.

68 G. A. Burdick, Phys. Rev. **129**(1), 138-50 (1963).

69 Z. Tang, M. Hasegawa, Y. Nagai, and M. Saito, Phys. Rev. B **65**(19), 195108 (2002).

70 M. Winter, WebElements: the periodic table on the WWW, www.webelements.com, 2016.

71 A. V. Generalov and A. S. Vinogradov, Phys. Solid State. **55**(6), 1136-47 (2013).

72 L. E. Orgel, J. Chem. Soc., 4186-90 (1958).

73 A. Gulans, J. Chem. Phys. **141**(16), 164127 (2014).